Ameloblastin Amphipathic Helix Motif mediates Ameloblast Polarization and Prismatic Enamel Formation via a RhoA Signaling Pathway

Gayathri Visakan[1], Rucha Arun Bapat[1], Jing Cai[1], Ethan Trevor Suwandi[2], Derk Joester[2], Natalie C Kegulian[1], Edwin Sarkisians[1], Marziyeh Aghazadeh[1], Simon Webster[1] and Janet Moradian-Oldak*[1]

1. Center for Craniofacial Molecular Biology, Herman Ostrow School of Dentistry of USC, University of Southern California, Los Angeles, CA, USA.

2. Department of Materials Science and Engineering, Northwestern University, Evanston, IL, USA

***Corresponding Author**

Janet Moradian-Oldak

joldak@usc.edu

Supplementary Information

Color Conservation Analysis

Ameloblastin protein sequences from mouse, pig and human were aligned using UniProt. The aligned FASTA sequences were analyzed for conservation using Color Conservation Analysis[1]. The threshold for identity and similarity was set at 100% and the amino acids were grouped as GAVLI, FYW, CM, ST, KRH, DENQ, P. Residues highlighted in black reveal identical residues and those in grey reveal similarity. Although the entire protein sequence was analyzed for conservation, the focus was on the AH motif contained within exon 5.

Plasmid design and protein expression and validation for recombinant mouse AmbnΔL76-P86

To generate the ΔL76–P86 deletion mutation in recombinant mouse Ambn, the previously used pET-32a plasmid expressing recombinant full-length mouse Ambn[2] was mutated using a pair of non-overlapping primers. One primer was designed to hybridize with the sense strand immediately 5’ to the 33 bases encoding the LNSLWLHGLLP amino acid sequence targeted for deletion, the other to hybridize with the antisense strand immediately 5’ to the 33 bases complementary to the bases encoding the above sequence. PCR, ligation, template removal, and transformation into NEB 5-alpha Competent *E. coli* (High Efficiency) cells were performed

using the Q5 Site-Directed Mutagenesis Kit (New England Biolabs, Inc.). Plasmid was purified using the QIAprep Spin Miniprep Kit (QIAGEN), sequenced by GENEWIZ from the T7 and T7-terminal ends to confirm successful incorporation of the ΔL76–P86 deletion, and transformed into BL21(DE3) *E. coli*, from which AmbnΔL76-P86 was expressed and purified as previously described.[3] Briefly, the *E. coli* cells were sonicated, protein affinity purified using Ni-NTA agarose columns (Qiagen). It was then dialyzed against 10kDa MWCO snakeskin dialysis membrane (Thermo) and purified using reverse phase HPLC (C4, Agilent) after removal of histidine, thioredoxin and S-tags using enterokinase (New England Biolabs) at 37℃. The protein was lyophilized overnight at -80℃ and stored in -20℃ until use. The new AH deletion mutant was characterized using 12% SDS-PAGE electrophoresis and Mass Spectrometry (ESI and MALDI). Mass spectrometry was carried out at Scripps Center for Mass Spectrometry and Metabolomics (San Diego, CA, USA).

Peptide design and synthesis

Ameloblastin peptide corresponding to the multitargeting domain (MTD), xAB2, and the peptide lacking LP region residues from the MTD, xAB2ΔL76-P86[1], were synthesized at Chempeptide Ltd. (Shanghai, China). Peptides were prepared as per previously published protocols[4] and used in cell spreading competition assays after reconstitution to 10 µg/ml in cell culture grade PBS (Gibco).

Transmission electron microscopy of recombinant proteins

Recombinant mouse Ambn, AmbnΔ5 and AmbnΔL76-P86, were purified and diluted to 20 µg/ml in 25 mM Tris-HCl (pH 7.4) and 150 mM NaCl. A 10 µl drop of the protein solution was applied to glow discharged carbon grids (400 mesh) and incubated for 5 minutes at room temperature. The grid was blotted using filter paper and immediately negatively stained with 2% uranyl acetate in double distilled water for 10 seconds (5 seconds for AmbnΔL76-P86), then blotted again and air dried. The grids were examined using transmission electron microscopy (Talos F200C G1 Biological TEM, FEI, OR, USA) with an accelerating voltage of 80 kV.

Dynamic Light Scattering analysis of recombinant proteins

Full-length recombinant mouse Ambn and recombinant AmbnΔL76-P86 were diluted individually to 3 µM in 50 mM Tris, 50 mM NaCl buffer at pH 7.6. Diluted samples were allowed to stand at room temperature for 1 h. Immediately prior to measurement, recombinant mouse Ambn was centrifuged for 5 min at 12,000 rpm to get rid of larger aggregates. No large aggregates were

observed in recombinant mouse AmbnΔL76-P86 and hence the mutant protein was not centrifuged. Samples were placed in a 10 µl quartz cuvette and measured at room temperature using a DynaPro NanoStar light scattering instrument (Wyatt). Ten acquisitions were performed with each being an average of ten scans for one experiment. Experiment was repeated at least three times with fresh dilution of protein prepared each time. Particle size distribution was reported as hydrodynamic radii based on a Rayleigh sphere model. For each curve showing particle size distribution, an intensity autocorrelation curve was simultaneously measured. Data were analyzed using Dynamics 7.1.1 and plotted in Microsoft Excel.

Optical microscopy

Both whole heads and hemi-mandibles from 7-week-old *Ambn*$^{WT/WT}$, *Ambn*$^{\Delta L76\text{-}P86\ +/-}$ and *Ambn*$^{\Delta L76\text{-}P86\ -/-}$ mice were examined under a dissecting microscope (Olympus, CKX53). Images were recorded for the examination of gross-enamel appearance of incisors (whole heads) and molars (dissected samples).

Enamel mineral density and thickness measurements from conventional micro-CT

Qualitative analysis of incisor enamel mineral density was carried out in three-dimensional sagittal reconstructions of mandibles from seven-week-old (7W) *Ambn*$^{WT/WT}$, *Ambn*$^{\Delta L76\text{-}P86\ +/-}$ and *Ambn*$^{\Delta L76\text{-}P86\ -/-}$ mice. Using heatmap renderings, incisor enamel mineral density along the sagittal plane was examined in the LP mutants and compared to WT. Commercial hydroxyapatite phantoms corresponding to mineral densities of 0.25 g/cm^3 and 0.75 g/cm^3 were used to calibrate the micro-CT system. An equation correlating mineral density and attenuation co-efficient was derived from the phantom scans and was used to measure mineral density of incisor enamel using the CTAn (software version 1.6.9.8; SkyScan). Four regions were identified on sagittal sections of incisors based on anatomical landmarks for measurement of enamel mineral density (Supplementary Figure 2). Relative enamel mineral density corresponding to regions 1-4 were obtained by normalizing against region 1 of *Ambn*$^{WT/WT}$ (corresponding to erupted enamel) and was plotted for the *Ambn*$^{\Delta L76\text{-}P86}$ mutants and *Ambn*$^{WT/WT}$ and absolute enamel mineral density values from region 4 (corresponding to erupted enamel) were analyzed and compared for statistical significance. 7W samples were used to measure and compare the enamel thickness. Five different samples were measured for enamel thickness at region 2 (which corresponds to the unerupted enamel). Heatmap rendering of axial incisor sections was used for measuring enamel thickness. Results were tabulated and analyzed for statistical significance.

High resolution micro-CT scanning and analysis using Convoluted Neural Networks

High resolution micro-CT scanning was performed at the Molecular Imaging Center at the Department of Radiology (University of Southern California, CA, USA) using a SCANCO µCT50 scanner with a polychromatic X-ray source that combines submicron pixel size (nanoCT), operating at 70 kV, 85 µA at an isotropic voxel size of 6µm. Mandibles were mounted on 3D printed custom holders, designed and generated at Northwestern University. High resolution reconstructions were segmented using convolutional neural networks (CNNs) performed at the Northwestern University (IL, USA) as per published protocols.[5] The reconstruction was normalized and converted to linear attenuation coefficient (μ) slice-wise along the longitudinal axis using the following equation:

$$\mu\,(i, j, k) = (I\,(i, j, k) - I_{bkg}).\,(\mu_{Al} - \mu_{bkg}) / (I_{Al} - I_{bkg})$$

where $I\,(i, j, k)$ is the intensity of the voxel with coordinates (i, j) in the k^{th} slice, I_{bkg} is mean grayscale value for the background class, I_{Al} is mean intensity for the aluminum wire, μ_{Al} is the linear attenuation coefficient of aluminum (1.706 cm^2/g)[6], and μ_{bkg} is assumed to have a value of 0 cm^{-1}. A convolutional neural network (CNN) with a 2D-to-2D U-Net architecture was used to segment reconstructions into one of the following eight classes: background (bkg), bone (bone), incisor enamel (IE), incisor dentin (ID), molar enamel (ME), molar dentin (MD), aluminum wire (Al) and ectopic mineral (EM). A manual clean-up was performed to correct misclassified volumes. Segmentation and clean-up were performed in Dragonfly 2022.0. All subsequent analysis was performed using custom scripts in MATLAB. After clean-up, additional algorithmic segmentation was performed to split the molar enamel and molar dentin classes into three subsequent subclasses representing the M1, M2, and M3 molars and identify pulp cavities in the incisor and the molars, and segment sockets and internal connective tissue A circle was then fitted to the dentino-enamel junction (DEJ) along the arc of the incisor (cervical-cuspal direction). Next, the arc length position of a selection of anatomical landmarks was determined. Arc length was defined as

$$L = r\theta$$

where r is the radius of the fitted circle and θ is the angle in radians. The position of the M1 distal root was defined as L = 0 for all samples.

Density (ρ) was calculated by the following relationship:

$$\rho = (\mu/\rho) / \mu$$

where (μ/ρ) is the mass attenuation co-efficient. The mass attenuation coefficient is a function of the material composition and source X-ray energy. A common approximation for polychromatic X-ray sources is to use the monochromatic coefficient at half the maximum source energy (27.5 keV). We used the mass attenuation coefficient of stochiometric hydroxyapatite (ρ = 3.16 g/cm^3, (ρ/μ) = 3.214 cm^2/g) to calculate mineralized tissue densities. Due to these approximations, the calculated density may underestimate the true density. Mineral mass is calculated as the product of the mineral density and the voxel volume. For the extraction of metrics as a function of arc length, the incisor is resampled between θ-z-planes spaced equidistantly along the fitted circle, typically at 10 μm intervals. Each wedge is also flattened as some metrics such as perimeters are more easily performed in 2D. Metrics include the maximum thickness measurements. To visualize the progression of density within the enamel body, density iso-surfaces are constructed by first performing as masked gaussian filter with a spatial standard deviation of σ = 9 μm on the incisor enamel to remove small islands and noise. The enamel was then partitioned into regions of 0.25 g.cm^3 in width. If the enamel is thick enough, voxels 15 μm from the enamel boundary are excluded to remove surface effects.

qPCR

Post-natal 5 days old (P5) molars, which are representative of secretory stage of amelogenesis were used. Enamel organ from mandibular molars (from 5 animals in each group) were dissected and RNA was extracted using RNeasy Plus Mini Kit (Qiagen) as per kit instructions. The extracted RNA was reverse transcribed using iScript Reverse Transcription Supermix for RT-qPCR (Bio-rad). The reverse transcribed cDNA from *Ambn*$^{WT/WT}$ and *Ambn*$^{\Delta L76\text{-}P86}$ mutants was used to determine the relative expression levels of *AmelX* and *Ambn* using CFX96 Real-Time System (Bio-rad) with iQ SYBR Green Supermix (Bio-rad). The primer sequences are outlined in Supplementary Table 1.

Bulk RNA sequencing

Ten enamel organs from five P5 pups of each genotype were pooled for RNA isolation. Efforts were made to ascertain that the pups in each group were from at least two different litters. RNA was isolated from the pooled tissue using RNeasy Plus mini kit (Qiagen 74134) according to manufacturer's instructions. Preliminary RNA quality check was performed using NanoDrop™ One Microvolume UV-Vis Spectrophotometer (Thermo Scientific, Catalog number ND-ONE-W). RNA samples with A260/280 ratio of approximately 2.0 and A260/230 ratio between 2.0-2.2 were used for further analysis. Second quality check was performed by Novogene using Agilent

Bioanalyzer. Only samples with RNA integrity number (RIN) > 7 were used for sequencing (n=3 for *Ambn*$^{\Delta L76\text{-}P86\ +/-}$ and *Ambn*$^{WT/WT}$, n=4 for *Ambn*$^{\Delta L76\text{-}P86\ -/-}$). RNA sequencing including mRNA library preparation (polyA enrichment) was performed by Novogene. The data were acquired using NovaSeq X Plus Series (PE150) sequencer at a sequencing depth of 20 million paired end reads. Data were analyzed using Partek Flow. Three or four samples per genotype of trimmed paired end reads were aligned to mouse genome GRCm39 (Gencode release M33) using STAR alignment and default parameters. Quantification was performed using Partek E/M algorithm with M33 annotation and strict paired-end compatibility. Genes with maximum counts <= 10 across all samples were filtered and normalization was performed using upper quartile normalization and 'add 1'. Since enamel matrix proteins or proteases of interest (Amelogenin, Ameloblastin, Enamelin, Odam, MMP20 and KLK4) did not appear as differentially expressed, raw normalized gene counts of each of the above genes were plotted to show their expression levels in *Ambn*$^{\Delta L76\text{-}P86}$ mutants and *Ambn*$^{WT/WT}$.

Immunofluorescent labeling of P8 incisors

For labeling of full-length Ambn, antigen retrieval was carried out overnight in citrate buffer (1mM sodium citrate dihydrate, pH 6.0) at 70℃. For all other immunolabeling experiments, slides were dehydrated for 1h at 60℃ in a hot air oven followed by rehydration in xylene (100%) and ethanol gradient (100%, 95%). Antigen retrieval was performed by boiling either in Tris-EDTA buffer (10 mM Tris Base, 1 mM EDTA, 0.05% Tween 20, pH 9.0) or citrate buffer (depending on antibody manufacturer's recommendations) for 22 mins at 100℃ followed by cooling for 22 mins. Endogenous peroxidases and enamel autofluorescence were blocked using 0.3% H_2O_2 treatment for 30 mins. Slides were blocked using 3% bovine serum albumin (BSA), 10% donkey serum and 0.05% Tween 20 for 2 h at room temperature. Slides were then incubated with primary antibody (diluted with 10% donkey serum and 0.05% Tween 20) overnight at room temperature in a moist chamber. Slides were incubated with secondary antibodies at room temperature in a moist chamber for 2 h, nuclei counterstained with 1:1000 DAPI and were mounted with Vectashield (Vector Laboratories) and coverslips were sealed with nail varnish.

Direct cell spreading assay using recombinant proteins and ameloblast lineage cells (ALC)

For direct spreading assay, established protocols for cell spreading competition assays were used with some modifications[7]. Briefly, 96-well plates (Cellstar) were coated with 100 µl of 10

μg/ml recombinant protein diluted in cell culture grade PBS (Gibco) overnight at 4℃. The following proteins were used: recombinant mouse Ambn or recombinant AmbnΔL76-P86. In the non-coated controls, wells were coated with PBS alone. The wells were blocked with 200 μl of 10 mg/ml heat denatured BSA for 1h at room temperature. ALC were trypsinized and resuspended in DMEM (without FBS) buffered with 20 mM HEPES at a cell suspension density of 1.0 x 10^4 cells/well. Cells were overlaid on wells with equal volume of 1X PBS and incubated at 37℃ for 90 mins. Cells were then fixed with 5% v/v glutaraldehyde, stained with 0.1% crystal violet and visualized using Keyence BZX710. The ratio of the number of cells that adopted a spread morphology to the total number of cells was determined by counting using ImageJ. The experiment was carried out in duplicates and repeated thrice.

ALC spreading competition assay using synthetic Ambn peptides

Established protocols for cell spreading competition assays were used.[7,8] 96-well plates (Cellstar) were coated with 100 μl of 10 μg/ml recombinant mouse Ambn overnight at 4℃. The plates were blocked with 200 μl of 10 mg/ml heat denatured BSA for 1h at room temperature. ALC were trypsinized and resuspended in DMEM buffered with 20 mM HEPES and allowed to incubate at 37℃ for 15 min at a resuspension density of 0.5 x 10^4 cells/well. The cells were treated with 10 μg/ml of xAB2 or xAB2ΔL76-P86 peptide or PBS. This mixture of cells and peptides was overlaid on the wells, and the plates were incubated at 37℃ for 90 min. The cells were fixed with 5% v/v glutaraldehyde and stained with 0.1% crystal violet and visualized with Keyence BZX710. The ratio of the number of cells that adopted a spread morphology to the total number of cells was determined using ImageJ. The experiment was carried out in duplicates and repeated thrice.

3D cell culture and aspect ratio measurements

Pre-chilled glass-bottomed 96-well plates (Mattek) were coated with 20 μg/ml test (recombinant mouse AmbnΔL76-P86) and control (heat denatured recombinant mouse Ambn, and WT recombinant Ambn) proteins. Ice-cold, growth-factor-reduced Geltrex (Thermo) was overlaid on coated plates and incubated at 37℃ for 30 min. ALC were detached from the culture dishes at 80% or greater confluence and were centrifuged at 200 x g for 5 mins to obtain a soft pellet. The cells were resuspended in cell culture media and inoculated atop set GFR Geltrex gels at a cell seeding density of 3.5 x 10^4 cells/well. Cells were allowed to attach to the gel for 30 mins at 37℃. Following cell attachment, a 10% v/v gel coat in cell culture media was overlaid on the cells to create a 3D-on-top-type culture. These 3D gels were incubated at in a standard cell

culture incubator for 24 h. At the end of the experiment, the cells were fixed with 25% glutaraldehyde for 15 min at room temperature. Cells in the 3D gel were labeled with 1:1000 DiD and 1:1000 DAPI and were visualized using Keyence BZX810 with objective PlanApo λ NA 0.75. Sequential Z stacks were recorded with a pitch of 0.4 μm. Z stacks were reconstructed using the Keyence Image Viewer (software version 1.1.1.8), and the 3D measure-tool was used to record the cell width along the XY plane and cell height along the Z axis. These values were tabulated, and the aspect ratio was calculated. Repeated measurements of aspect ratio were recorded to analyze for statistical significance, and the experiments were repeated three times.

Supplementary Table 1

AmelX	F- GTCACCTCTGCATCCCATG
	R- TTCCCGCTTGGTCTTGTC
Ambn	F- CTGTTACCAAAGGCCCTGAA
	R- GCCATTTGTGAAAGGAGAG

Supplementary Table 1. Primer sequences for qPCR for amelogenin *(AmelX)* and ameloblastin *(Ambn)*

Supplementary Figure 1

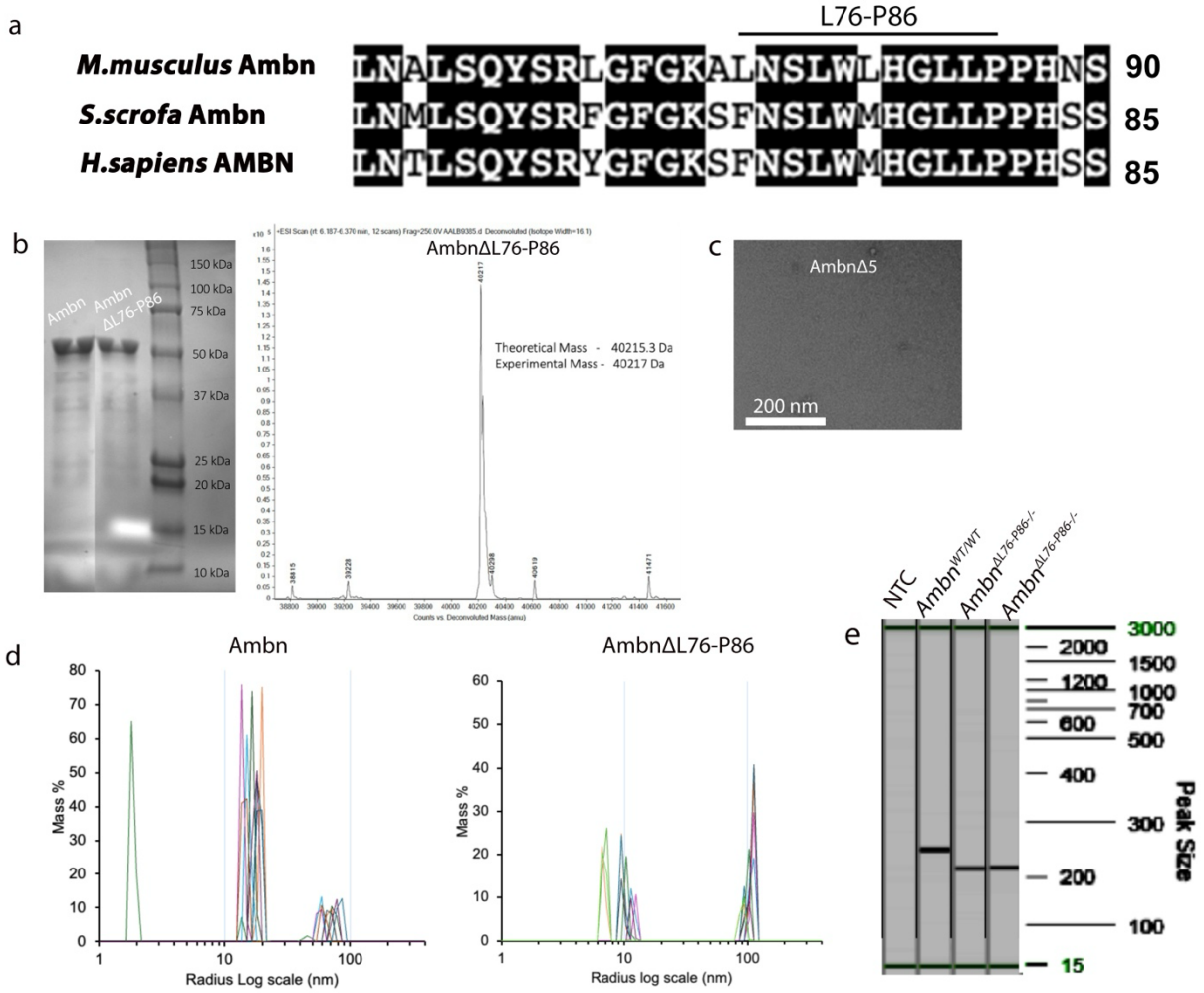

Supplementary Figure 1. Rationale for design of Ambn$^{\Delta L76\text{-}P86}$ mutants. (**a**) Color Conservation Analysis of ameloblastin amphipathic helix motif region from representative mammals. Residues highlighted in black show 100% sequence identity. The LP region spanning from Lys76 - Pro86 is highlighted on the top. (**b**) Characterization of recombinant mouse LP deletion mutant protein using 12% SDS PAGE electrophoresis (left) and Mass Spectrometry ESI analysis (right). (**c**) Transmission electron microscopy analysis of recombinant mouse AmbnΔ5 protein showing lack of self-assembly. (**d**) Dynamic Light Scattering (DLS) of recombinant mouse Ambn (left) and recombinant mouse AmbnΔL76-P86 (right). (**e**) Agarose gel electrophoresis of *Ambn*$^{\Delta L76\text{-}P86}$ mutants. One male and female sample are shown. Genotyping analysis performed at UC Davis.

Supplementary Figure 2

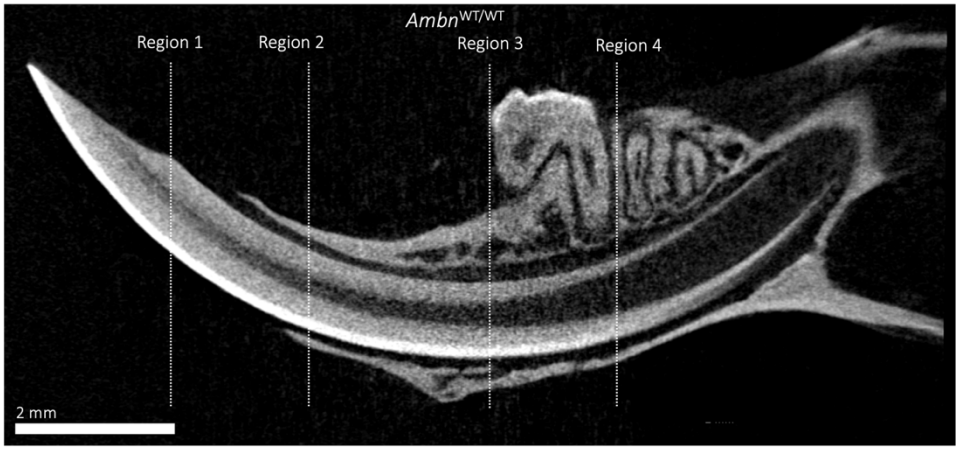

Supplementary Figure 2. Sagittal reconstruction of seven-week-old mandible from showing anatomical landmarks used for enamel mineral density measurements.

Supplementary Figure 3

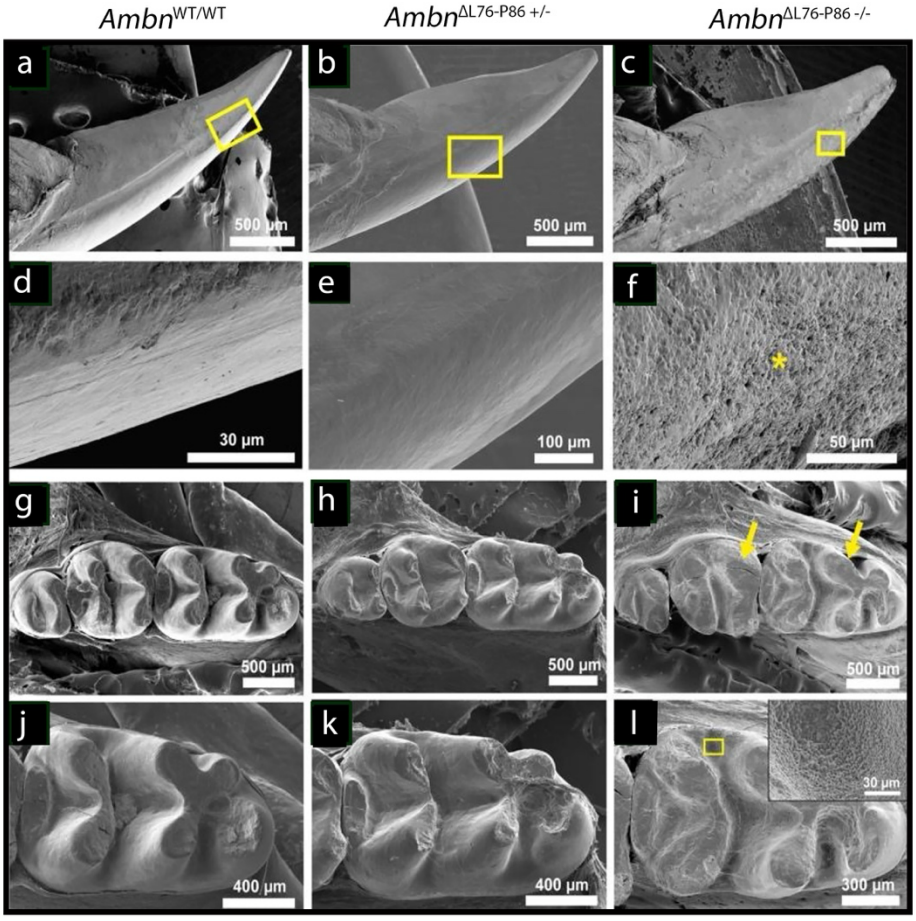

Supplementary Figure 3. Scanning electron microscopy analysis of 7-week-old incisors (top two panels) and molars (bottom two panels) from *Ambn*$^{WT/WT}$ and *Ambn*$^{\Delta L76\text{-}P86}$ mutants. (**a - c**) Low resolution images from the labial surface of incisors from *Ambn*$^{WT/WT}$ (a), *Ambn*$^{\Delta L76\text{-}P86\ +/-}$ (b), and *Ambn*$^{\Delta L76\text{-}P86\ -/-}$(c). Yellow squares indicate the locations from where high-resolution images were recorded. (**d - f**) High resolution images from the labial surface of incisors from *Ambn*$^{WT/WT}$ (d), *Ambn*$^{\Delta L76\text{-}P86\ +/-}$ (e), and *Ambn*$^{\Delta L76\text{-}P86\ -/-}$ (f). (**g - i**) Low resolution

images from the occlusal surface of molars from *Ambn*$^{WT/WT}$ (g), *Ambn*$^{\Delta L76\text{-}P86\ +/-}$ (h), and *Ambn*$^{\Delta L76\text{-}P86\ -/-}$(i). Yellow arrows in I indicate significant wear of occlusal tips of molars resulting in a flat occlusal plane in *Ambn*$^{\Delta L76\text{-}P86\ -/-}$ mutants. (**j - l**) High resolution images from the occlusal surface of molars from *Ambn*$^{WT/WT}$ (j), *Ambn*$^{\Delta L76\text{-}P86\ +/-}$ (k), and *Ambn*$^{\Delta L76\text{-}P86\text{-}/-}$ (l). Inset in L shows increased surface roughness on the slopes of the molar cusps in *Ambn*$^{\Delta L76\text{-}P86\ -/-}$.

Supplementary Figure 4

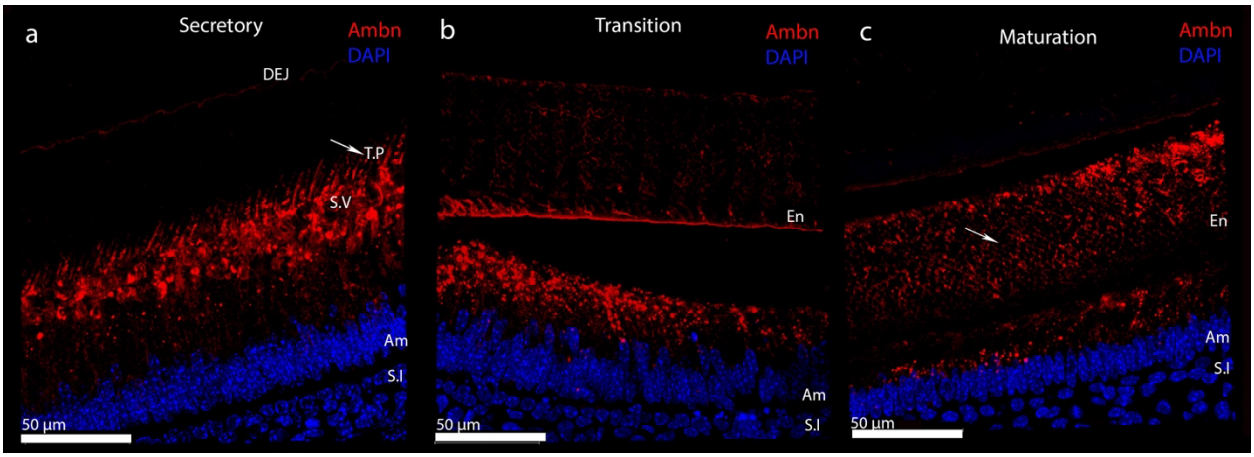

Supplementary Figure 4. (a - c) Custom N-terminal Ambn peptide antibody characterization using stagewise immunolabeling of post-natal 8-day old incisors from *Ambn*$^{WT/WT}$ in secretory stage (a), transition stage (b) and maturation stage (c) of amelogenesis. T.P- Tomes' Processes, S.V- secretory vesicles, Am- ameloblast, S.I stratum intermedium,

Supplementary Figure 5

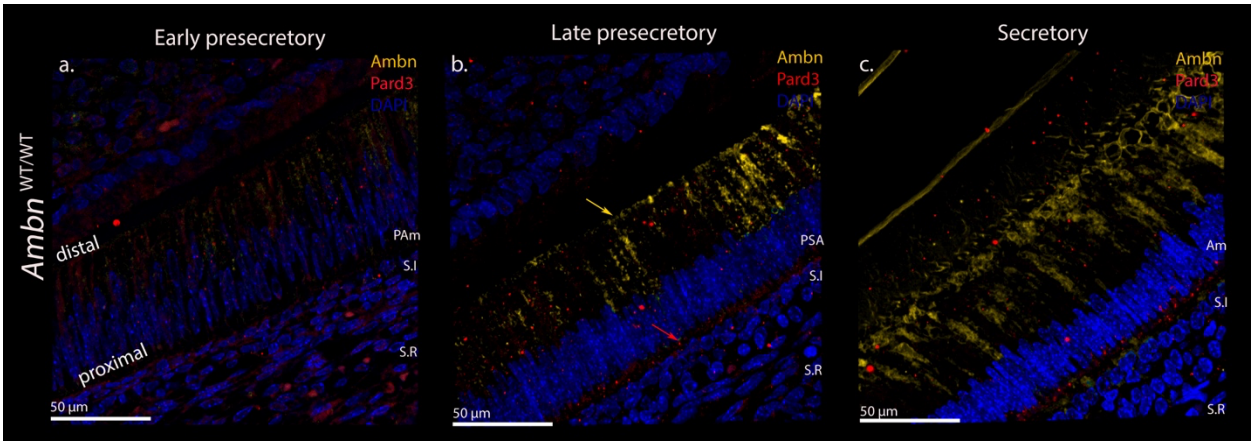

Supplementary Figure 5. Custom N-terminal anti-Ambn antibody co-labeling with anti-β-actin antibody in secretory stage. (**a - d**) Secretory stage incisors from *Ambn*$^{WT/WT}$ co-labeled with N-terminal anti-Ambn antibody and anti-β-actin. (**e - h**) Secretory stage incisors from *Ambn*$^{\Delta L76\text{-}P86\ -}$

$^{/-}$ mutant co-labeled with N-terminal anti-Ambn antibody and β-actin. Co-labeling of N-terminal anti-Ambn antibody with anti-β-actin shows specific labeling along the distal ameloblast membrane and Tomes' Processes in *Ambn*$^{WT/WT}$ (b - d). In the case of the *Ambn*$^{\Delta L76\text{-}P86\ -/-}$ mutant, this membrane localization of N-terminal anti-Ambn antibody is lost (f - h). nucleus (blue), actin (green), Ambn (red).

Supplementary Figure 6

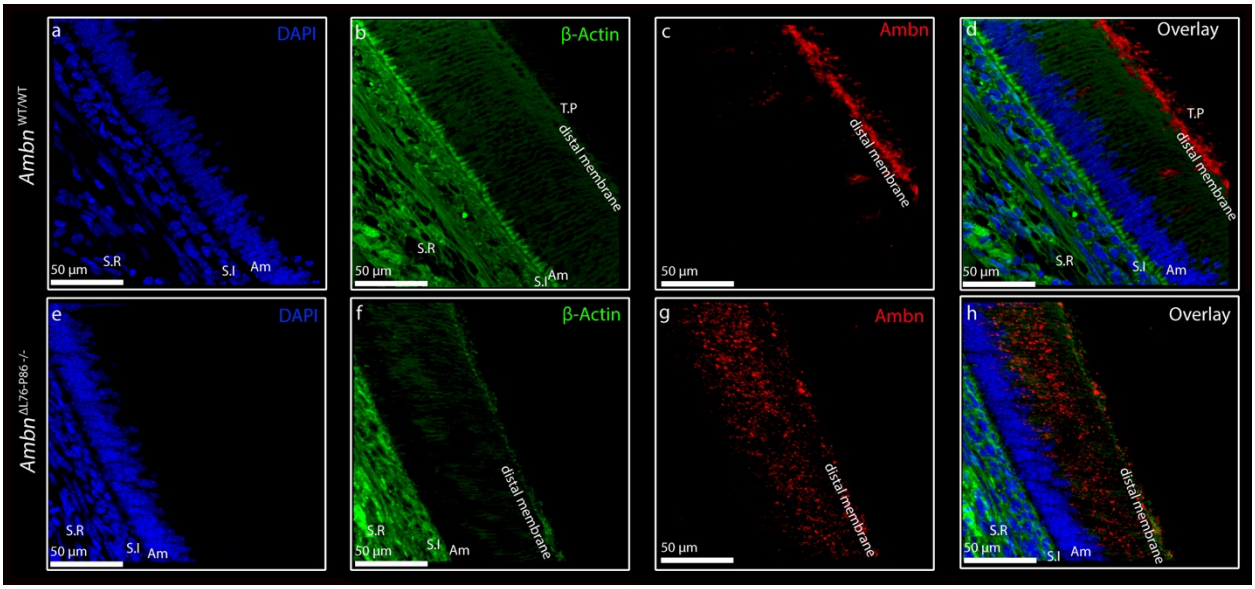

Supplementary Figure 6. (**a - c**) Stagewise immunolabeling of P8 secretory stage incisors from *Ambn*$^{WT/WT}$ mice for Pard3 (red) and full-length Ambn (yellow pseudo-color). Red arrow in B indicates the onset of a polarized Pard3 immunolocalization within the presecretory ameloblasts and yellow arrow in B indicates prominent Ambn immunoreactivity along the distal ameloblast cell membrane. PAm- Pre-ameloblast, PSA- presecretory ameloblast, T.P- Tomes' Processes, Am- ameloblast, S.I stratum intermedium, S.R stellate reticulum.

Supplementary Figure 7

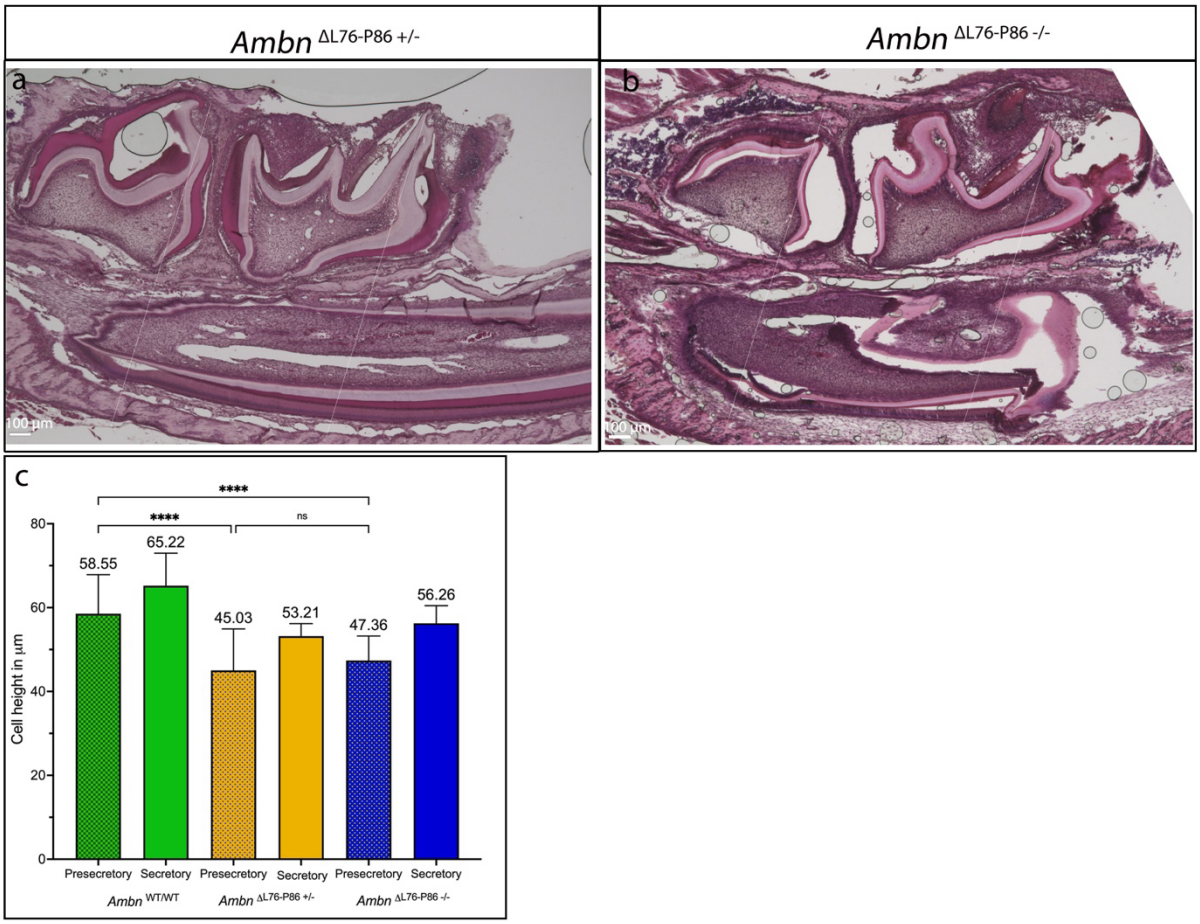

Supplementary Figure 7. (**a, b**) Anatomical landmarks used to identify secretory and presecretory stages of amelogenesis along a continuously growing incisor. (**c**) Presecretory versus secretory stage ameloblast height measurements from *Ambn*$^{WT/WT}$ and *Ambn*$^{\Delta L76\text{-}P86}$ mutants. *Ambn*$^{WT/WT}$ (green), *Ambn*$^{\Delta L76\text{-}P86\ +/-}$ (yellow) *and Ambn*$^{\Delta L76\text{-}P86\ -/-}$ (blue). * $p < 0.05$; ** $p < 0.01$, *** $p < 0.001$, n/s- not significant.

Supplementary Figure 8

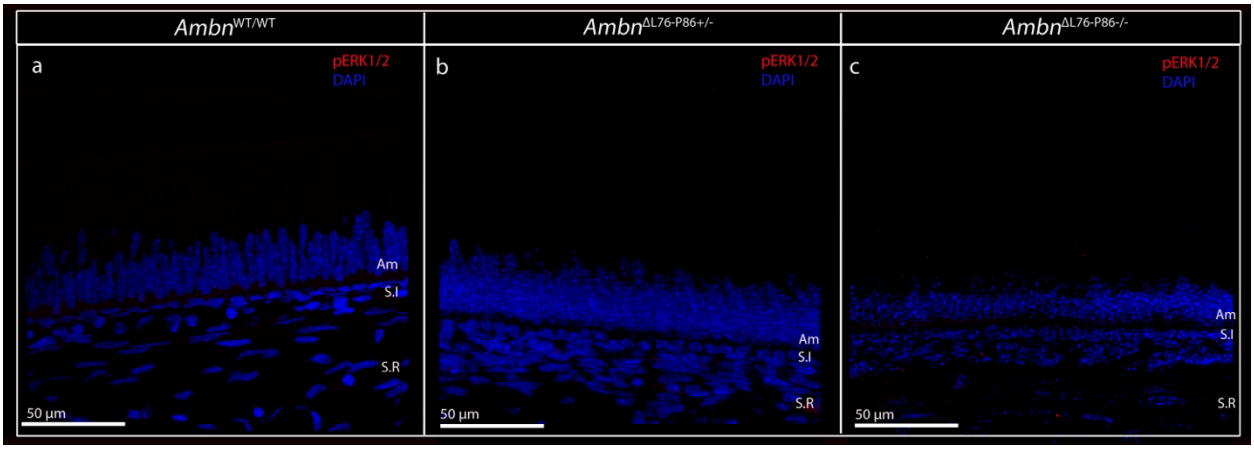

Supplementary Figure 8. (**a**) Immunolabeling for MAPK pathway mediator, p-Erk 1/2 in secretory stage ameloblasts of *Ambn*$^{WT/WT}$.(**b**) Immunolabeling for p-Erk 1/2 in in secretory stage ameloblasts of *Ambn*$^{\Delta L76\text{-}P86\ +/-}$. (**c**) Immunolabeling for p-Erk 1/2 in in secretory stage ameloblasts of *Ambn*$^{\Delta L76\text{-}P86\ -/-}$.

Supplementary Figure 9

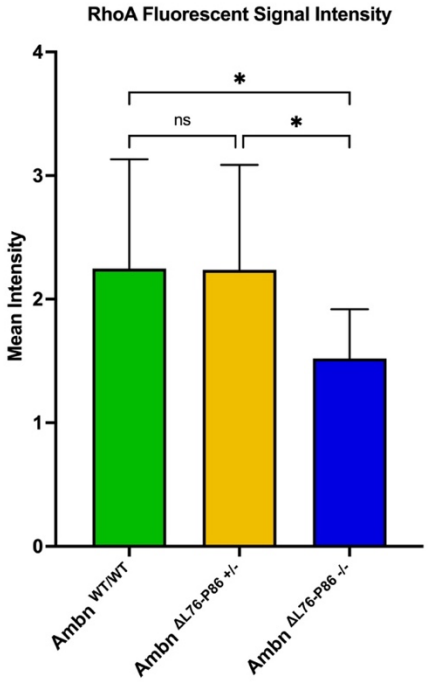

Supplementary Figure 9. Mean signal intensity comparison between *Ambn* $^{WT/WT}$ and *Ambn*$^{\Delta L76\text{-}P86}$ mutants for anti-RhoA antibody. *Ambn* $^{WT/WT}$ (green), *Ambn*$^{\Delta L76\text{-}P86\ +/-}$ (yellow) and *Ambn*$^{\Delta L76\text{-}P86\ -/-}$ (blue). * $p < 0.05$.

References

1 Kegulian, N. C. & Moradian-Oldak, J. Deletion within ameloblastin multitargeting domain reduces its interaction with artificial cell membrane. *J. Struct. Biol.* **216**, 108143 (2024).

2 Su, J., Kegulian, N. C., Bapat, R. A. & Moradian-Oldak, J. Ameloblastin binds to phospholipid bilayers via a helix-forming motif within the sequence encoded by exon 5. *ACS omega* **4**, 4405-4416 (2019).

3 Su, J., Bapat, R. A. & Moradian-Oldak, J. in *Odontogenesis* 229-236 (Springer, 2019).

4 Kegulian, N. C., Langen, R. & Moradian-Oldak, J. The dynamic interactions of a multitargeting domain in ameloblastin protein with amelogenin and membrane. *Int. J. Mol. Sci.* **24**, 3484 (2023).

5 Cooley, V. *et al.* in *Developments in X-Ray Tomography XIII.* 28 (SPIE).

6 Hubbell, J. H. & Seltzer, S. M. Tables of X-ray mass attenuation coefficients and mass energy-absorption coefficients 1 keV to 20 MeV for elements Z= 1 to 92 and 48 additional substances of dosimetric interest. (National Inst. of Standards and Technology-PL, Gaithersburg, MD (United …, 1995).

7 Humphries, M. J. Cell adhesion assays. *Extracellular Matrix Protocols: Second Edition*, 203-210 (2009).

8 Su, J., Bapat, R., Visakan, G. & Moradian-Oldak, J. An Evolutionarily Conserved Helix Mediates Ameloblastin-Cell Interaction. *J. Dent. Res.*, 0022034520918521 (2020).